JOURNAL OF GEOPHYSICAL RESEARCH, VOL. 106, NO. C1, PAGES 859–877, JANUARY 15, 2001

Modeling salinity distributions in the Indian Ocean

Weiqing Han
Program in Atmospheric and Oceanic Sciences, University of Colorado, Boulder, Colorado

Julian P. McCreary Jr.
International Pacific Research Center, University of Hawaii, Honolulu, Hawaii

Abstract. A $4^1/_2$-layer model with active thermodynamics and mixed-layer physics is used to isolate effects on salinity distributions in the Indian Ocean that result from various forcing mechanisms. These forcings include evaporation ($\mathcal{E}$) and precipitation ($\mathcal{P}$) through the ocean surface and inflows across basin boundaries by river runoff in the Bay of Bengal, the Indonesian Throughflow, the Persian Gulf, and the Red Sea. A suite of solutions is obtained in which each forcing is added sequentially. In the solution forced only by $\mathcal{P} - \mathcal{E}$, salinity patterns in the upper three layers agree qualitatively with the observations, but values tend to be higher throughout most of the basin. When river inflow into the Bay of Bengal is included, salinity values are significantly improved in the upper three layers, especially in the northern Bay and along the east and west coasts of India. In addition, solutions suggest that during the Northeast Monsoon part of the river water flows out of the Bay in the shallow channel between Sri Lanka and India: Only when this channel is opened in the upper layer do solutions develop a strong, across-shelf salinity gradient along the west Indian coast, consistent with the observations. When the Indonesian Throughflow is added, salinities are lowered in all four layers, especially in the southern tropical ocean. Most of the Throughflow eventually flows out of the Indian Ocean along the western boundary and near Madagascar, but some is advected across the equator by the East African Coastal Current, where it is carried eastward and northward into the central Arabian Sea. Saltier Persian Gulf Water is introduced into the model in layer 3. Some of it subsequently entrains into the surface mixed layer, increasing sea surface salinity by 0.1–0.2 practical salinity units (psu) in a broad region of the Arabian Sea. Saltier Red Sea Water enters the basin in layer 4. It increases layer 4 salinity values throughout much of the Indian Ocean, particularly in the Somali Basin, the interior Arabian Sea, and the central and western equatorial ocean.

1. Introduction

Precipitation $\mathcal{P}$ and evaporation $\mathcal{E}$ are major causes of salinity variations in all the oceans. In the Indian Ocean, salinity distributions are also driven by river inflow primarily in the Bay of Bengal, the influx of fresher water in the Indonesian Throughflow, and the influx of saltier waters from the Red Sea and Persian Gulf. Plate 1 plots bimonthly maps of sea surface salinity (SSS; *Levitus and Boyer* [1994]), superimposed with arrows of ship drift currents [*Mariano et al.*, 1995]. The combined influences of the fresh water sources in the eastern ocean (rainfall, rivers, and the Indonesian Throughflow) are apparent in the panels.

Copyright 2001 by the American Geophysical Union.

Paper number 2000JC000316.
0148-0227/01/2000JC000316$09.00

In this paper, we use a general circulation model (GCM) of intermediate complexity (a $4^1/_2$-layer system) to assess how each of these forcing mechanisms affects Indian Ocean salinity distributions. (In a companion paper (*Han et al.* [2000], hereinafter referred to as HMK) we discuss how two of them, $\mathcal{P} - \mathcal{E}$ and river inflow, affect upper ocean dynamics, thermodynamics, and mixed-layer physics.) The model's simplicity is an advantage in that it is computationally efficient and allows for processes to be readily diagnosed. At the same time it is sophisticated enough to develop solutions that compare well with observations, often remarkably so, an indication that the model properly represents the fundamental physics at work in the region. For example, solutions are able to reproduce the annual variability of observed upper ocean currents, sea surface temperature (SST), and mixed-layer thickness in much of the Indian Ocean (see HMK).

To isolate effects due to each forcing, we obtain a hierarchy of solutions, adding one more forcing at each

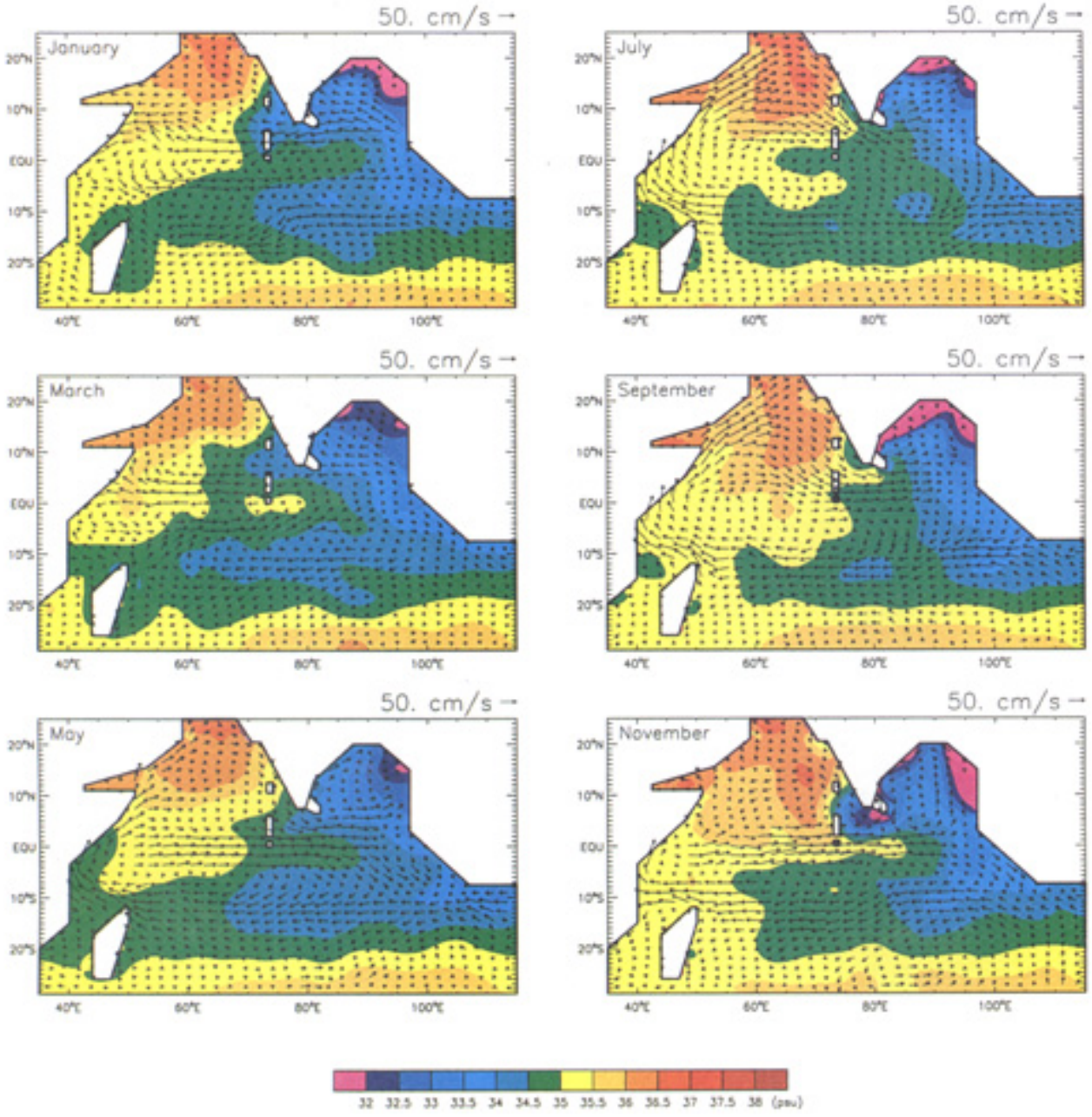

Plate 1. Bimonthly plots of SSS [*Levitus and Boyer*, 1994] and ship drift currents [*Mariano et al.*, 1995].

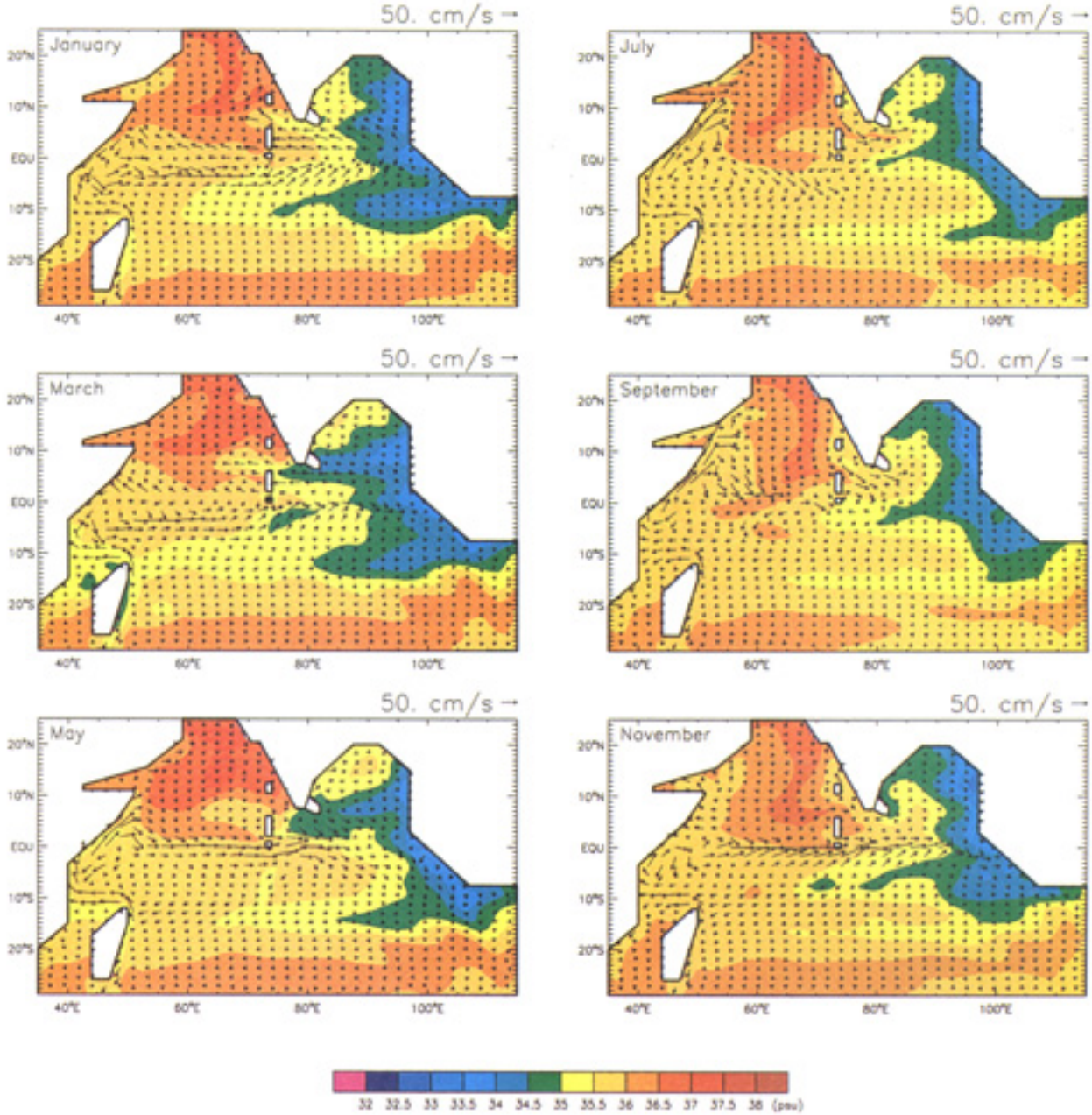

Plate 2. Bimonthly plots of S_1 and $\mathbf{v}_1$ fields from solution TR1.

step. As we shall see, each forcing is needed to obtain salinity distributions that compare well with observations.

2. Ocean Model

The model is described in detail by *Han* [1999] and *Han et al.* [1999], and descriptions of similar versions of the model are given by *McCreary et al.* [1993] (hereinafter referred to as MKM). Here, then, we only describe its aspects that are most pertinent to the present study.

Figure 1 illustrates the model's structure. It consists of four active layers with thicknesses h_i (i = 1–4 is a layer index), temperatures T_i, salinities S_i, and velocities $\mathbf{v}_i = (u_i, v_i)$, overlying a deep, quiescent ocean with temperature T_d and salinity S_d where pressure gradients are assumed to vanish (the "1/2" layer). The w_i terms are velocities at the bases of layers 1–3 that specify how water transfers across the interfaces between the layers. Velocity w_1 is essentially determined as in the *Kraus and Turner* [1967] mixed-layer model, and w_2 primarily relaxes $h_1 + h_2$ back to a prescribed thickness (65 m) to parametrize the process of subduction (see MKM). This subduction process is not allowed to happen within the equatorial band of 5°S to 5°N, as given by *Han et al.* [1999]. Velocity w_3 is included to keep h_3 from being thinner than $h_{3\min} = 50$ m. In addition, w_1 and w_2 contain "correction" terms that act only to prevent layers from becoming thinner than prescribed values, $h_{1\min} = h_{2\min} = 10$ m. The T_i and S_i fields are allowed to vary in response to both surface forcing and across-layer transfer by the w_i fields, so that the layers are not isopycnal ones. Given the parameterizations of the w_i, it is more appropriate rather to interpret them as corresponding to distinct water mass types, namely, the surface mixed layer, seasonal thermocline, thermocline, and upper intermediate water in layers 1–4, respectively.

The salinity equation in each layer is

$$S_{it} + \mathbf{v}_i \cdot \nabla S_i - \kappa_s \nabla^2 S_i + \kappa_{s4} \nabla^4 S_i = -\delta_{i1}(\mathcal{P} - \mathcal{E}) S_1 / h_1 + w_i^+ (S_{i+1} - S_i)/h_i - w_{i-1}^- (S_{i-1} - S_i)/h_i + \delta_{i3}\gamma_s (S_4 - S_3)/h_3 + \delta_{i4}\gamma_s (S_3 - 2S_4 + S_d)/h_4, \quad (1)$$

where $\kappa_s = 10^7$ cm^2/s and $\kappa_{s4} = 10^{21}$ cm^4/s are coefficients of Laplacian and biharmonic mixing, velocities $w_i^+ = \max(w_i, 0)$ and $w_i^- = \min(w_i, 0)$ are the positive and negative parts of w_i, $\gamma_s = 3.3 \times 10^{-4}$ m/d is a diffusion coefficient, $\mathcal{E}$ is evaporation, $\mathcal{P}$ is precipitation, δ_{ij} is a Kronecker delta function (δ_{ij} is 1 if $i = j$ and is 0 otherwise), and it is assumed that $w_0 = w_4 = 0$. According to equation (1), salinity variations are affected by horizontal advection and mixing, $\mathcal{P} - \mathcal{E}$, entrainment from the underlying layer (the term proportional to w_i^+), detrainment from the overlying layer (the term proportional to w_{i-1}^-), and vertical mixing between layer 3 and layer 4, and between layer 4 and the deep ocean (the terms proportional to γ_s). Physically, the γ_s terms represent property exchanges due to weak, background diapycnal mixing.

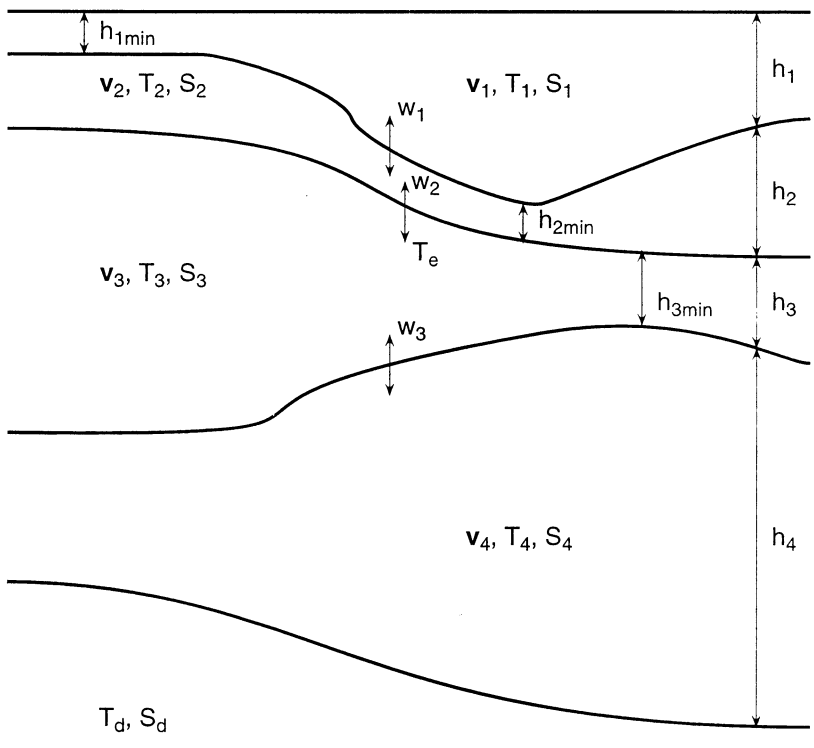

Figure 1. A schematic diagram illustrating the layer structure of the 4½-layer model.

The model basin is a simplified representation of the Indian Ocean north of 29°S, and it is shown in many of the figures and plates that display solutions. All continental and island (Sri Lanka, Madagascar, Maldives, and Lakshadweep Islands) boundaries are vertical walls, and no-slip boundary conditions are applied there. Exceptions are for solutions that allow exchange across boundaries (sections 4–7). In addition, Sri Lanka has two configurations: one with Sri Lanka completely attached to the Indian continent and the other with it detached in layer 1 (section 4.3).

The southern boundary is open. Zero-gradient conditions are applied there, except when there is inflow into layers 3 and 4; in that case, the waters that enter the basin are specified to have temperatures of 15°C and 8°C and salinities of 35.6 and 34.8 psu, respectively. In addition, there is a damper on the u_i fields near the boundary in order to eliminate numerical instabilities (see MKM).

The precipitation data set of *Legates and Willmott* [1990] is used to force the model. A description of the other surface forcing fields (wind stress and heat fluxes) is given by *Han et al.* [1999] and MKM. The model is also forced by exchanges across basin boundaries, and they are described in sections 4–7.

The horizontal resolution of the grid is $\Delta x = \Delta y = 55$ km and the time step is $\Delta t = 0.8$ hours. Other numerical details are given in MKM, *Han* [1999], and *Han et al.* [1999]. The model is spun up from a state of rest beginning on April 15, a time during the transition between the monsoons when the winds are weak. The model is integrated for a period of 60 years, by which time solutions approach equilibrium. All solutions displayed in later sections are from year 60.

3. Precipitation and Evaporation

In this section, we describe the salinity distributions in a solution forced only by $\mathcal{P} - \mathcal{E}$ (solution TR1). This solution lies at the bottom of our hierarchy, and the other forcings are added sequentially in sections 4–7.

3.1. Forcing

Figure 2 shows the $\mathcal{P} - \mathcal{E}$ field during January (top panel) and July (bottom panel) for solution TR1. Because of the intense rainfall in the central and eastern equatorial ocean, precipitation exceeds evaporation ($\mathcal{P} - \mathcal{E} > 0$) throughout the year. Significant precipitation occurs near Madagascar from January to May, and there is intense rainfall near the west coast of India and the eastern boundary of the Bay of Bengal during the Southwest Monsoon, resulting in the positive $\mathcal{P} - \mathcal{E}$ in these regions. In contrast, in the Arabian Sea and southern tropical ocean where rainfall is weak, evaporation is in excess of precipitation ($\mathcal{P} - \mathcal{E} < 0$) during most of the year.

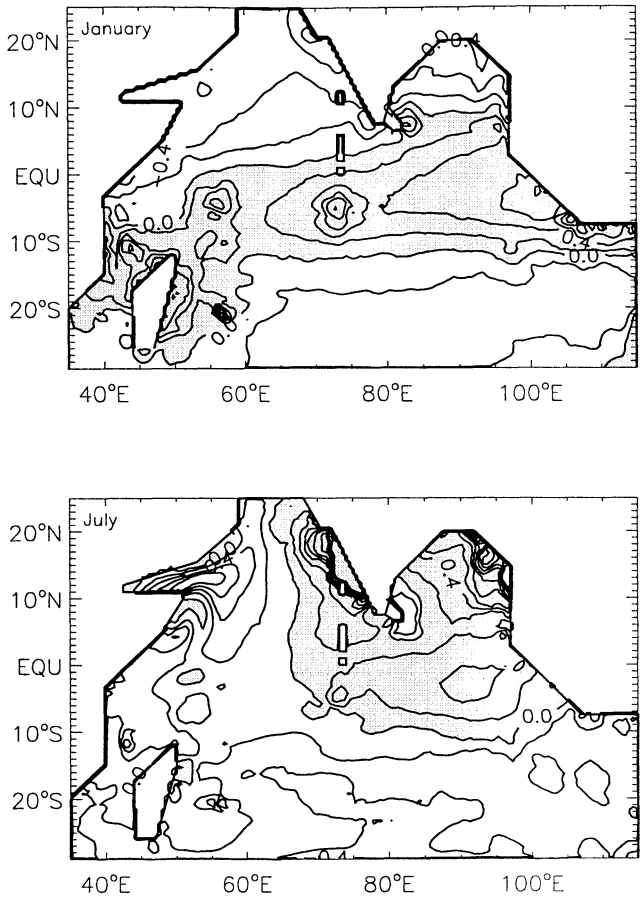

Figure 2. Precipitation $\mathcal{P}$ minus evaporation $\mathcal{E}$ (cm/d) during (top) January and (bottom) July from solution TR1. Contour interval is 0.2 cm/d. Positive values are shaded.

3.2. Sea Surface Salinity

Plate 2 shows bimonthly mixed-layer salinity S_1 and $\mathbf{v}_1$ fields from solution TR1. Generally, positive $\mathcal{P} - \mathcal{E}$ forces low S_1 in the eastern ocean north of about 15°S throughout the year, around Madagascar from January to March, and along the west coast of India during the Southwest Monsoon (Figure 2). In contrast, negative $\mathcal{P} - \mathcal{E}$ produces high S_1 elsewhere, especially in the northern Arabian Sea and the southern tropical ocean (Figure 2). These S_1 patterns are qualitatively consistent with the observed SSS field (Plate 1). The magnitude of S_1, however, is generally 0.5–1 psu higher than observed SSS in most parts of the ocean. In particular, S_1 is 2–4 psu saltier in the Bay of Bengal and along the west coast of India. These high values suggest that fresh waters from rivers and the Indonesian Throughflow are necessary for producing a realistic SSS field, and this idea is confirmed in sections 4 and 5.

Although S_1 generally follows the $\mathcal{P} - \mathcal{E}$ pattern, basin-wide water mass exchange is evident in both the model solution and the observations. For example, a prominent feature in plates 1 and 2 is a broad, eastward stretching, high-salinity tongue in the equatorial

ocean generated by the spring and fall Wyrtki Jets (WJs; *Wyrtki* [1973]), which carry saltier water from the western basin to the east. Low-salinity water in the eastern equatorial ocean also pushes westward during the Southwest Monsoon, forming a narrow, low-salinity tongue. In the southern tropical ocean the South Equatorial Current (SEC) tends to carry fresher water westward out of the eastern basin.

In the northern Indian Ocean, fresher Bay of Bengal water enters the Arabian Sea in two ways: by the southward flowing East India Coastal Current (EICC) from October to December, and by the southward flowing eastern branch of the anticyclonic gyre present in the Bay from February to May. In the latter case, this fresher water is subsequently advected westward by the Northeast Monsoon Current (NMC) into the Arabian Sea (March and May panels of Plate 2). The eastern branch also removes fresher water from the Bay by advecting it to, and across, the equator (see section 4.2).

Conversely, salty Arabian Sea Water (ASW) also flows into the Bay of Bengal. One important conduit of this flow is the Southwest Monsoon Current (SMC), which carries ASW eastward and then northward into the Bay during the summer and fall [*Vinayachandran et al.*, 1999], producing a salty tongue south of India and east of Sri Lanka (July and September panels in Plate 2). To a lesser extent, the northward flow associated with the eastern branch of the cyclonic gyre in the Bay during the Northeast Monsoon carries part of the saltier water from the southern Bay northward; in this case, the source of the salty water is eastward transport from the Arabian Sea by the fall WJ (November panel of Plate 2).

3.3. Subsurface Salinities

The S_2 field (not shown) has a similar pattern to that of S_1, because the two layers are so strongly mixed by entrainment and detrainment processes and because they have similar current patterns. An exception during the Southwest Monsoon happens because of the absence of surface Ekman drift in layer 2; as a consequence, in the Bay of Bengal salty ASW advects farther north in layer 2 than it does in layer 1, and fresher Bay of Bengal water advects more southward in layer 1 than in layer 2.

Subduction due to w_2 is the primary reason for S_3 variation (Figure 3). As a consequence, S_3 is high in the Arabian Sea and the southern tropical ocean, where strong seasonal subduction introduces the saltier water into the thermocline; it is low in the Bay of Bengal and in the Southern Hemisphere from 5°S to 15°S across the Indian Ocean because relatively fresh surface water subducts into layer 3 in these regions. In comparison to observed salinity at 200 m (bottom panel of Figure 3), S_3 tends to be 0.5–1 psu saltier throughout the ocean, a discrepancy that is reduced when rivers and the Indonesian Throughflow are included (sections 4 and 5).

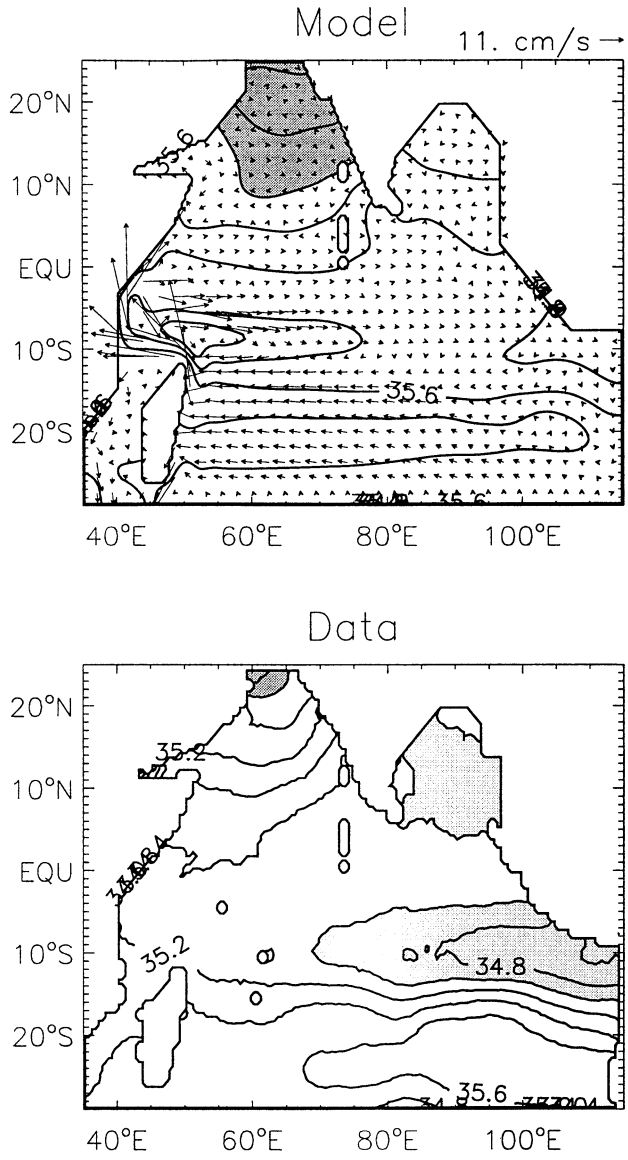

Figure 3. (top) Annual mean S_3 and $\mathbf{v}_3$ fields from solution TR1 and (bottom) annual mean salinity at 200 m from the *Levitus and Boyer* [1994] data. The contour interval for S_3 is 0.2 psu. Salinity values greater than 36 psu have dark shading, and values less than 35 psu have light shading.

The S_4 field (not shown) has little variation because weak vertical diffusion by the γ_s term is the only process that can alter S_4. As will be discussed in sections 5 and 7, significant S_4 variations happen only when inflows from the Indonesian Throughflow and Red Sea are taken into account.

4. River Inflow

In this section, we examine the salinity variations due to inflow from the Bay of Bengal rivers. These rivers include the Ganges-Brahmaputra, the Irrawaddy, and other smaller rivers along the east coast of India that we collectively refer to as "local" rivers.

4.1. Forcing

The Ganges-Brahmaputra river annually discharges approximately 10^{12} m^3 of fresh water into the northern Bay of Bengal. Figure 4 plots the monthly mean climatology of the Ganges-Brahmaputra river transport $R(t)$ [*United Nations Educational, Scientific, and Cultural Organization (UNESCO)*, 1972, 1974, 1979, 1988; *Shetye*, 1993]. Most of the discharge ($\gtrsim$70%) occurs during the Southwest Monsoon from June through October [*Martin et al.*, 1981; *Shetye*, 1993; *Shetye et al.*, 1996]. The Irrawaddy river, located in the northeastern Bay along the coast of Burma, is the second-largest river in the Bay with an annual discharge approximately 40% of that from the Ganges-Brahmaputra (S. Shetye, personal communication, 1996). Other rivers are significantly weaker.

The Ganges-Brahmaputra river is included in the model by specifying an inflow of layer 1 water into the basin and an outflow of layer 2 water along a segment of the northern boundary, a boundary exchange that simulates an overturning circulation driven by vertical mixing within the adjacent estuary. Along the boundary segment, 88°E $\leq x \leq$ 90°E, y = 20°N, we set

$$v_1 = -\frac{M_1}{h_1 L_r}, \quad S_1 = S_{1\mathrm{in}}, \quad v_2 = \frac{M_2}{h_2 L_r}, \tag{2a}$$

where $L_r = 2°$ is the width of the segment, M_1 and M_2 are the inflow and outflow transports, respectively, and $S_{1\mathrm{in}}$ is the salinity that emerges from the river mouth. The value of $S_{1\mathrm{in}}$ is set to 21 psu, not completely fresh because of the mixing of river and ocean waters within the estuary; its value lies between the minimum salinity observed from hydrographic data during the Southwest Monsoon (16 psu; *Murty et al.*, [1992]) and the minimum SSS value from the *Levitus and Boyer* [1994] data during September (24 psu). Mass and salt conservation requires that

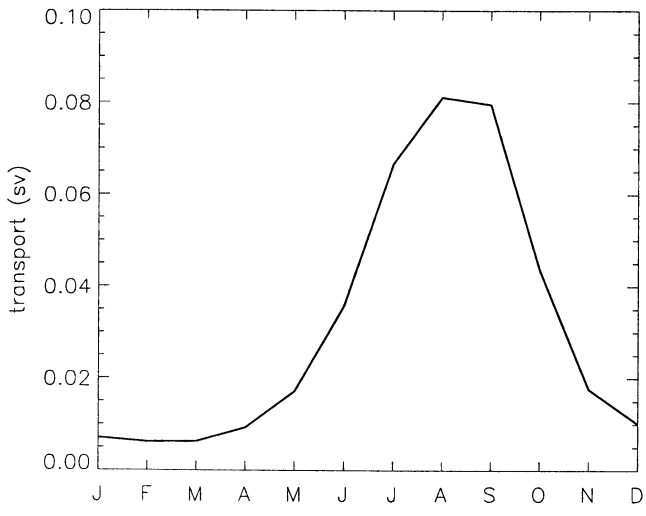

Figure 4. Monthly mean climatology of transport from the Ganges-Brahmaputra river.

$$M_1 - M_2 = R(t), \qquad M_1 S_1 = M_2 S_2, \tag{2b}$$

where S_2 is the value of layer 2 salinity adjacent to the river mouth. Transports M_1 and M_2 are determined by solving this pair of equations.

The Irrawaddy river is included along the boundary segment, 94.5°E $< x <$ 96.5°E, 17°N $> y >$ 15.5°N, by the same procedure. Its transport is chosen to be $0.1R(t)$, less than the value of $0.4R(t)$ suggested from climatological data. We used this smaller transport because S_1 became too fresh in test solutions driven by the larger one. A possible reason for this problem is that $\mathcal{P}$ overestimates rainfall near the eastern boundary of the Bay, by interpolating strong land precipitation during the Southwest Monsoon onto the adjacent ocean. The inflow salinity $S_{1\mathrm{in}}$ for the Irrawaddy river is specified to be 23 psu, a value higher than that for Ganges-Brahmaputra because of its smaller transport and, hence, presumed greater estuarine mixing.

The local rivers included in the model are the Mahanadi (88°–89.5°E, 20°N), Godavari (83.5°–84.5°E, 16°–17°N), Krishna (82.5°–83.5°E, 15°–16°N), and Kaveri (80.5°E, 10.5°–11.5°N). Their transports are taken from the climatology [*UNESCO*, 1972, 1974, 1979, 1988] except for river Kaveri, whose transport is not available in the data; its transport is assumed to be $0.1R(t)$, a value similar to that of Krishna river. Inflow salinities $S_{1\mathrm{in}}$ are specified to be 21 psu for the Mahanadi because it is adjacent to the Ganges-Brahmaputra in our model, 28 psu for the Godavari and Krishna rivers because of their smaller transports, and 24 psu for the Kaveri since the observations show a relative low SSS there during the Southwest Monsoon [*Levitus and Boyer*, 1994, Plate 1; *Donguy and Meyers*, 1996].

4.2. Sea Surface Salinity

Plate 3a plots bimonthly maps of S_1 and $\mathbf{v}_1$ for a solution driven by inflow from only the Ganges-Brahmaputra and Irrawaddy rivers as well as by $\mathcal{P} - \mathcal{E}$ (solution TR2). In the Bay of Bengal, the river inflow reduces S_1 by 1–10 psu, producing a pattern in much better agreement with the observations throughout the Bay (compare Plates 3a and 1). Adjacent to the river mouths, however, salinity values are considerably fresher in the solution than they are in the data. This discrepancy may not be a model error, but may rather happen because the data are insufficient in this region and are highly smoothed. In support of this idea, hydrographic observations [*Murty et al.*, 1992] show a low-salinity value of 16 psu near the mouth of Ganges-Brahmaputra during the Southwest Monsoon, even lower than the minimum salinity of 21.7 psu in our solution; moreover, S_1 values agree well with in situ observations of SSS elsewhere in the Bay during both monsoons [Figure 9 of *Shetye et al.*, 1996; Figure 4a of *Murty et al.*, 1992].

During the summer and early fall (May–September panels of Plate 3a), river water remains in the north-

eastern portion of the Bay because the coastal currents are either convergent (May) or weak. In the first part of the Northeast Monsoon (October–January) the EICC reverses direction to flow southward along the east coast of India, consistent with the observed circulation (Plate 1; *Shetye* [1993]), and carries some of the fresh water with it. Later in the season (February–May) a basin-wide anticyclonic gyre forms, again consistent with the observed flow (Plate 1; *Shetye* [1993]), and advects the fresh water southward along the eastern boundary and into the central Bay.

The southward EICC that brings river water to the southern tip of India from October to January merges with the NMC and enters the Arabian Sea (November panel of Plate 3a). There, most of it is trapped within the Lakshadweep High (LH), an anticyclonic circulation that forms off the southwest coast of India during the Northeast Monsoon (January panel of Plate 3a). The LH propagates westward as a Rossby wave during spring [*Shankar and Shetye*, 1997], and it carries the fresher water into the interior Arabian Sea (January and March panels of Plate 3a). As it moves across the Arabian Sea, it mixes with saltier layer 2 water, and only a weak low-S_1 signal ever reaches the Somali coast.

Very little Bay of Bengal water is advected northward along the west coast of India in solution TR2. This property contrasts with the observed SSS field, which shows a strong across-shelf salinity gradient there during the winter (compare November and January panels of Plates 3a and 1, Figure 1b of *Shetye et al.* [1991], and Figure 15 of *Donguy and Meyers* [1996]). It is noteworthy that SSS in Plate 1 attains its lowest value near the southern tip of India and south of Sri Lanka during November, whereas solution TR2 does so during December. As discussed in section 4.3, this one-month delay is the likely reason for the model-data discrepancy. As a result, river water arrives at the tip of India after the LH forms and becomes trapped within it, and hence little of it is able to advect up the coast. Processes that hasten its arrival in our model are discussed in section 4.3.

Another important pathway for removing river water from the Bay is the southward flow along the eastern boundary of the Bay during the late spring and summer. This current carries some of the river water to the equator, where part of it is subsequently advected westward by the equatorial flow during summer and another part is carried southward across the equator (July and September panels in Plate 3a). In the southern tropical ocean the SEC then advects the fresher water westward across the basin near 15°S, where a small portion of it is advected northward by the East African Coastal Current (EACC; May panel), and the rest flows out of the Indian Ocean near Madagascar and the western boundary (January–May panels). River water decreases SSS in the equatorial and southern tropical ocean by 0.1–1 psu (compare Plates 3a and 1).

4.3. Local Rivers and India-Sri Lanka Separation

As noted in section 4.2, river water advected by the EICC arrives at the tip of India too late to be carried farther north by the northward flowing West India Coastal Current (WICC) in the late fall. There are two possible ways to shorten the arrival time: increasing the speed of the EICC and shortening the river water pathway along the east coast of India. Because the speed of the EICC in solution TR2 is consistent with the observations (see HMK), reducing the length of the river water pathway seems to be the more realistic possibility. This can be done by including local rivers along the east coast of India and by allowing exchange through the shallow channel that separates India and Sri Lanka. Indeed, the distribution of the observed SSS field indicates the probable influence of both effects (Plate 1). Low SSS along the east coast of India from 10°N to 13°N throughout the year reflects the influence of river Kaveri, which forms a delta before entering the Indian Ocean (D. Shankar, personal communication, 1999). The minimum SSS during November happens south of India and Sri Lanka rather than east of Sri Lanka, supporting the idea of direct exchange through the India–Sri Lanka channel.

To test the influence of local rivers and the India–Sri Lanka separation, Plate 3b plots November and January maps for three test solutions. They differ from solution TR2 in that local rivers are added (solution TR2A, top panels), there is an India–Sri Lanka separation (solution TR2B, middle panels), and both local rivers and the India–Sri Lanka separation are included (solution TR2C, bottom panels). India and Sri Lanka are separated by several shallow ($\lesssim$10 m) passages, most notably "Adam's Bridge" and the Pamban Pass. To simulate these passages, the shape of Sri Lanka is altered as shown in the middle and bottom panels of Plate 3b, the separation consisting of two grid boxes (100 km width). Exchange is allowed to occur only in layer 1, the flows in layers 2–4 being blocked by a line barrier at 9.5°N.

In solution TR2A (top panels) most of the river water is still trapped within the LH, although during November the fresher water front does advance 2° farther to the west and SSS is lower at the southern tip of India. The blocking of the fresh water at the tip of India results from the eastward flowing SMC, which is adjacent to the southern Sri Lankan coast through October. It is not until November that the currents south of Sri Lanka reverse direction, and fresher Bay of Bengal water begins to be advected westward there. In solution TR2B (middle panels) a significant amount of river water does reach the southern tip of India directly through the passage, but most is still trapped within the LH because water from the Ganges-Brahmaputra and Irrawaddy rivers has such a long pathway to reach the southern tip of India.

In solution TR2C (bottom panels) the river water passes through the separation in October and surrounds the southern tip of India in November, agreeing well with the observed distribution at that time (Plate 1). Some of this large accumulation of fresher water is then able to be advected northward by the WICC during November and December, producing a strong across-shelf salinity gradient along the west coast of India in better agreement with the observations (compare Plate 3b with corresponding panels of Plate 1 and with Figure 1b of *Shetye et al.* [1991] and Figure 15 of *Donguy and Meyers* [1996]).

Unfortunately, there is no scientifically reliable evidence that supports the existence of the channel flow in solution TR2C. There is, however, an anecdotal description of flow through the Pamban Pass given by United Kingdom Hydrographic Office [1975, page 80] (S. Shetye, personal communication, 1998), which states

> In 1958, there was a least depth of 2.1 m in the pass and maximum draught of vessels using it was 3.2 m ··· Tidal Streams are only noticeable at the change of the Monsoon in March, April, and October; other times they are masked by the south-going current during the Northeast Monsoon and by the north-going current during the Southwest Monsoon, these often attain rates of 6 knots, making passage of the pass difficult even for powered vessels.

How consistent is the channel flow in solution TR2C with this description? Assume that the passages in the actual India-Sri Lanka separation sum to a width of 20 km and have an average depth of 5 m. Then, with a peak current speed of 6 knots (~300 cm/s), the transport is 0.3 Sv. In solution TR2C at 9.5°N during November, h_1 is ~27 m thick, the peak current speed is ~37 cm/s, and so with a current width of 100 km the transport through passage is 1 Sv. This comparison suggests that the passage flow is overestimated in the model. It is also noteworthy that solution TR2C does not have the strong northward flowing channel current during the Southwest Monsoon alluded to by the United Kingdom Hydrographic Office, for reasons that are not clear.

4.4. Subsurface Salinities

The S_2 field (not shown) agrees very well with observed salinity values at 50 m in the Bay of Bengal during the Southwest Monsoon [Figure 4b of *Murty et al.*, 1992]. It has a similar pattern to S_1, and its change due to adding the rivers is also similar to S_1, owing to the active mass exchange between, and the similar current patterns within, layers 1 and 2. An exception is near the southern tip and west coast of India during fall and winter, where little fresher water flows directly from the Bay into these regions. Reasons for this difference are that the EICC and WICC are considerably weaker in layer 2, the layer 2 currents south of Sri Lanka are eastward until November, and the India-Sri Lanka separation is closed in the subsurface layers.

Figure 5 shows the annual mean S_3 field from solution TR2C. The most striking change from solution TR1 is the decrease in S_3 throughout the Bay of Bengal, where S_3 is 0.1–0.4 psu fresher than in TR1, in much better agreement with the data (compare the panels of Figures 5 and 3). In the southern tropical ocean near 15°S, S_3 is also reduced by 0.1–0.2 psu from its values in solution TR1. These S_3 decreases result from subduction by w_2 of the fresher, river water into the thermocline layer in solution TR2C, since it is the only process by which layer 3 receives water from upper layers (see equation (1)). Changes in S_3 are very weak in the equatorial ocean (5°S to 5°N) because no subduction is allowed there. In contrast, the S_4 field remains almost unchanged because vertical diffusion of salinity, the only process by which river water can affect S_4, is very weak.

5. Indonesian Throughflow

5.1. Forcing

The net flow of fresher waters from the Pacific to the Indian Ocean through the Indonesian Archipelago, the Indonesian Throughflow, has been detected both by direct current measurements [*Murray and Arief*, 1988] and by indirect estimates from hydrography [*Wyrtki*, 1961; *Fieux et al.*, 1994; *Meyers et al.*, 1995; *Bray et al.*, 1996]. Estimated transports vary from an annual mean value of 2 Sv in the upper 200 m [*Wyrtki*, 1961] and 5 Sv in the upper 300–400 m [*Meyers et al.*, 1995; *Fine*, 1985] to 22 Sv above 500 m during the peak of the Southeast Monsoon [*Fieux et al.*, 1994].

To include the Indonesian Throughflow in the model, we specify a westward current across the eastern boundary segment, $x = 115°E$, $9°S \leq y \leq 16°S$, by replacing

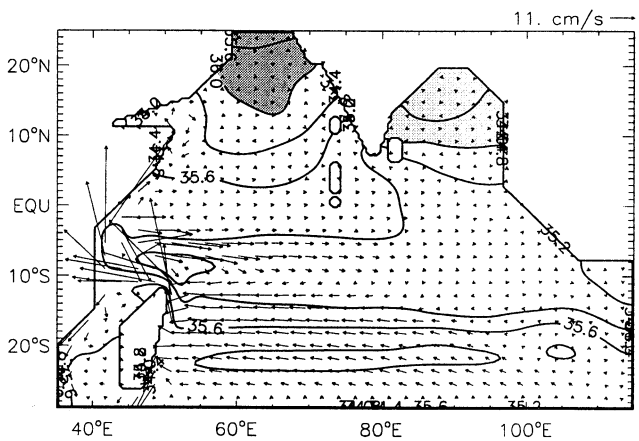

Figure 5. Annual mean S_3 and $\mathbf{v}_3$ fields from solution TR2C. The contour interval for S_3 is 0.2 psu. Salinity values greater than 36 psu have dark shading, and values less than 35 psu have light shading.

the closed conditions on u_i, S_i, and T_i with

$$u_i = -\frac{U_i}{h_i L_f}, \qquad S_i = S_i^*, \qquad T_i = T_i^*, \qquad (3)$$

where U_i = (5, 2, 2, 1) Sv, S_i^* = (33.8, 34.3, 34.7, 34.5) psu, T_i^* = (28.5, 27, 16, 7.2)°C, and $L_f = 7°$ is the width of the segment. These values are suggested either from the above observations or from previous modeling studies [*Miyama et al.*, 1995, 1996]. Our specification assumes that the Throughflow transport is time independent. Solutions forced by annually varying transports produce salinity patterns very similar to the ones reported here in the interior Indian Ocean.

5.2. Sea Surface Salinity

Plate 4 shows bimonthly maps of S_1 for the solution forced as in solution TR2C and also by the Indonesian Throughflow (solution TR3). The addition of the Throughflow reduces S_1 by 0.2–2 psu in a broad region of the Southern Hemisphere, especially from 10°S to 25°S across the Indian Ocean and near the southwestern boundary of the basin (compare Plates 3a and 4). To a lesser extent, the Throughflow decreases S_1 by 0.2–0.4 psu in the Somali Basin, western Arabian Sea, and at some locations in the Bay of Bengal. These changes considerably improve the S_1 field in the southern tropical ocean and southern Arabian Sea, making it agree better with observed SSS (Plate 1).

Consistent with previous observational and modeling studies [*Godfrey and Golding*, 1981; *Fine*, 1985; *Gordon*, 1986; *Godfrey*, 1989; *Kundu and McCreary*, 1986; *MKM*; *Hirst and Godfrey*, 1993; *Haines et al.*, 1999], almost all the Throughflow waters are advected westward across the Indian Ocean by the SEC, except for a small amount that flows southward along the west Australian coast via the Leeuwin Current (compare Plates 3a and 4). The westward flowing Throughflow water drifts southward because of the southward Ekman flow present in the surface mixed layer.

After the Throughflow water arrives at the western ocean most of it flows out of the Indian Ocean along the western boundary and near Madagascar, again consistent with previous research. A significant amount, however, is advected northward by the northward flowing EACC at the western boundary (Plate 4). This water then bifurcates near 2°S, with one branch heading eastward into the ocean interior and the other directing northward into the Arabian Sea along the Somali coast. The swift Somali Current then carries the Throughflow water into the Arabian Sea during the Southwest Monsoon . During other seasons the South Equatorial Countercurrent (SECC) (January–March) and the WJs (spring and fall) carry the Throughflow water eastward into the central and eastern ocean (Figure 4). A very small amount of Throughflow water is carried into the Bay of Bengal by the SMC and by the eastern branch of the cyclonic gyre in the Bay during the Northeast Monsoon.

Tracers for the Throughflow waters exhibit the same pathways as discussed above, but with a clearer pattern (not shown). Interestingly, they show that there is no direct pathway by which Throughflow water can enter the Bay of Bengal along the eastern boundary of the basin. This is because there are no northward currents that flow across the equator in the eastern ocean, and horizontal mixing, which could cause northward spreading, is overwhelmed by westward advection.

5.3. Subsurface Salinities

As for the preceding solutions, changes of S_2 caused by the Throughflow (not shown) are similar to those of S_1 because of the strong mixing and similar current patterns in the two layers. In layer 3 (Figure 6a), the Throughflow decreases S_3 by 0.2–0.8 psu in the southern tropical ocean across the Indian Ocean and by 0.2–0.4 psu along the Somali coast as well as near 10°–15°N of the western Arabian Sea. For the rest of the ocean the decrease of S_3 is small (compare Figures 5 and 6a). The resultant S_3 field agrees much better with the *Levitus and Boyer* [1994] data (bottom panel of Figure 3). Pathways for the Throughflow waters in layers 2 and 3 are similar to those in the surface mixed layer, because of the active water mass exchanges and similar current patterns in all the layers. These pathways are consistent with the ones demonstrated by *Haines et al.* [1999].

The S_4 field is freshened by 0.1–0.3 psu only in the southeastern ocean especially near the Throughflow entrance, and it hardly changes at all in the rest of the basin (not shown). This confined structure happens because an extremely weak interior current (~0.3 cm/s) is generated by the boundary transport U_4. This property is in obvious contrast to the Levitus data at 600 m (bottom panel of Figure 6b), which has a low-salinity band (34.4–34.8 psu) extending across the southern tropical ocean. This model-data discrepancy suggests that ei-

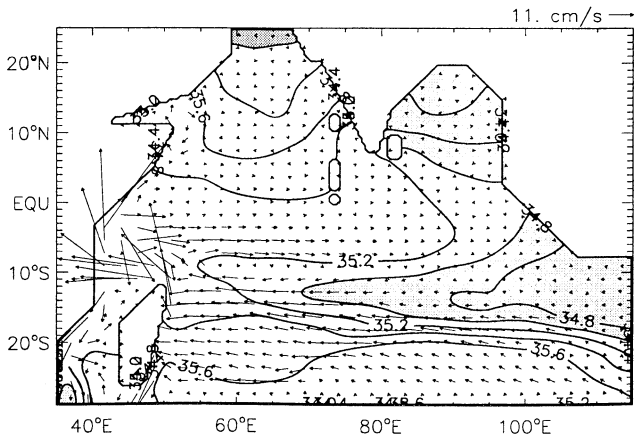

Figure 6a. Annual mean S_3 and $\mathbf{v}_3$ fields from solution TR3. The contour interval of S_3 is 0.2 psu. Salinity values less than 35 psu have light shading, and those greater than 36 psu have dark shading.

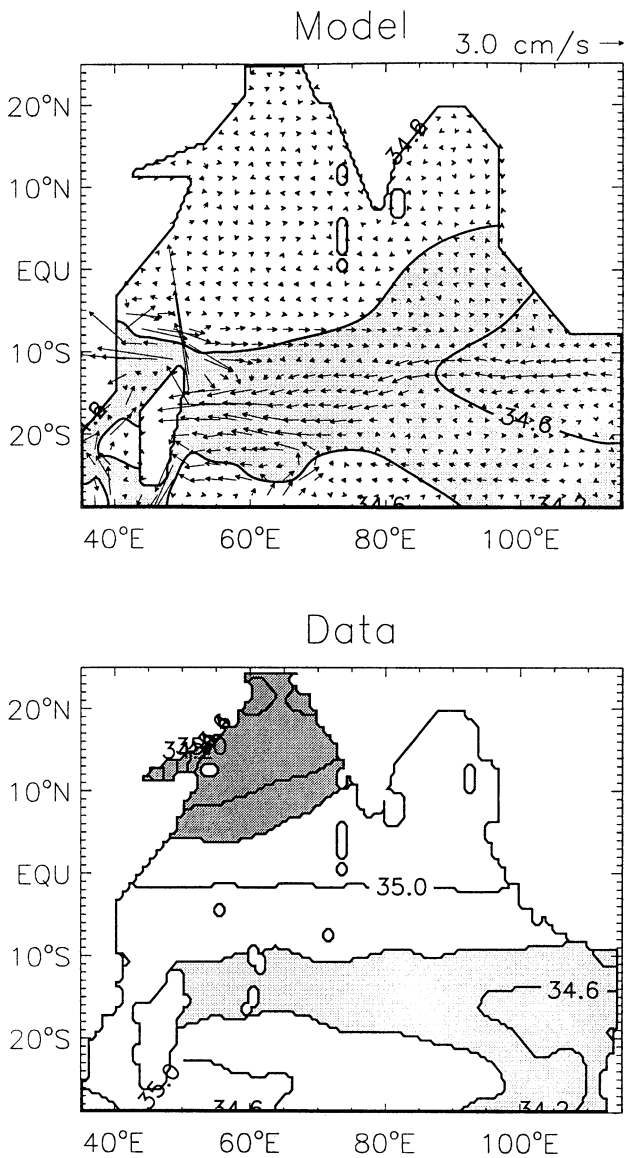

Figure 6b. (top) Annual mean S_4 and $\mathbf{v}_4$ fields from solution TR3A and (bottom) annual mean salinity at 600 m from the *Levitus and Boyer* [1994] data. Salinity values higher than 35.2 psu have dark shading, and those lower than 34.8 psu have light shading.

ther a larger Throughflow transport is needed in layer 4 or that horizontal mixing is too strong in our model.

To produce a better salinity pattern in this layer, we increased U_4 to 6 Sv (solution TR3A). In this solution the low-salinity tongue stretches westward into the central and western ocean because of strengthened advection, in much better agreement with the *Levitus and Boyer* [1994] data (compare the panels of Figure 6b). This improvement supports the idea that a significant amount of Throughflow water enters the Indian Ocean in the intermediate layer, a conclusion consistent with the observations of deep flow through the Timor Passage reported by *Molcard and Fieux* [1996]. Another evident model-data difference in Figure 6b is the higher salinity throughout the Northern Hemisphere in the data, especially in the Arabian Sea. This discrepancy suggests that the salty Red Sea Water is needed to produce a realistic layer 4 salinity field (see section 7).

In layer 4, horizontal mixing is as important as advection for spreading the Throughflow waters, because currents are typically so weak (<2 cm/s; upper panel of Figure 6b). As a consequence, although Throughflow water flows westward across the southern tropical ocean with most of it flowing out of the Indian Ocean in the southwestern region, a large part also spreads over the entire basin because of horizontal mixing, especially into the equatorial ocean and the Bay of Bengal.

6. Persian Gulf

6.1. Forcing

Highly saline water is generated within the Persian Gulf by strong evaporation. After leaving the Gulf this water sinks and mixes with the surrounding waters in the Gulf of Oman, forming a layer of Persian Gulf Water (PGW; 21°C, 37.5 psu) at depths of 200–300 m [*Reynolds*, 1994]. After it enters the Arabian Sea the core layer of PGW is observed at depths of 250–300 m with a density of $\sigma_t = 26.7$ [*Wyrtki*, 1971; *Quadfasel and Schott*, 1982; *Morrison and Olson*, 1991].

To introduce PGW into the model, we allow an exchange flow between the Gulf of Oman and the Indian Ocean. Specifically, we modify the boundary conditions along the boundary segment, $x = 59°\text{E}$ and $22°\text{N} \leq y \leq 25°\text{N}$, to be

$$u_3 = \frac{M_3}{h_3 L_\text{p}}, \quad S_3 = S_{3\text{in}},$$

$$T_3 = T_{3\text{in}}, \quad u_1 = -\frac{M_1}{h_1 L_\text{p}}, \tag{4}$$

where $S_{3\text{in}} = 37$ psu, $T_{3\text{in}} = 18°\text{C}$, and $L_\text{p} = 3°$ is the width of the segment. The value of M_3 is specified according to the numerical solution of *Chao et al.* [1992], which reaches a peak of 0.15 Sv in March and a low of 0.02 Sv in August and September. The surface outflow transport M_1 is then determined from the salt balance equation across the boundary segment

$$M_3 S_3 = M_1 S_1. \tag{5}$$

In this specification, $S_{3\text{in}}$ and $T_{3\text{in}}$ are lower than the values suggested by the observations (37.5 psu and 21°C). This inflow, therefore, is representative of PGW after it has mixed with the ambient waters in the Gulf of Oman, just before it enters the Indian Ocean.

6.2. Salinities

Figure 7a shows the annual mean S_3 field for the solution forced as in solution TR3A but also with a prescribed inflow of PGW (solution TR4). Figure 7b shows

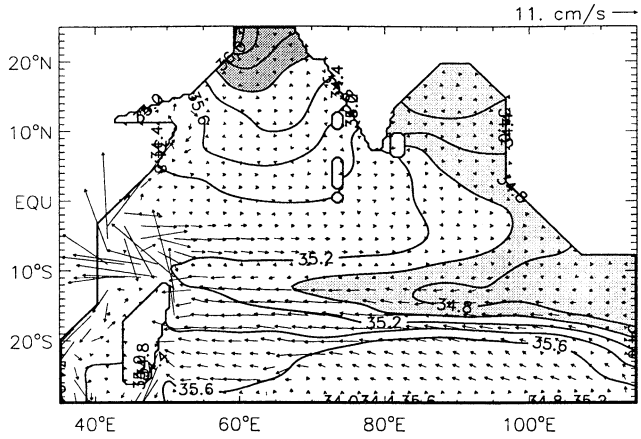

Figure 7a. Annual mean S_3 and $\mathbf{v}_3$ fields from solution TR4. The contour interval for S_3 is 0.2 psu. Values less than 35 psu have light shading, and those greater than 36 psu have dark shading.

salinity fields from the difference solution, TR4 – TR3A, and currents from solution TR4 in layers 3 and 1 during July.

In solution TR4, S_3 increases by 0.1–0.6 psu in the northern Arabian Sea (Figure 7a and upper panel of Figure 7b), producing a salinity pattern in much better agreement with the observations, especially with strong S_3 gradients near the Gulf of Oman (compare corresponding panels of Figures 7a, 6a, and 3). The S_1 field also increases by 0.1–0.2 psu in a broad region of the northern Arabian Sea (lower panel of Figure 7b), bringing S_1 even closer to observed SSS (compare corresponding panels of Figure 7b and Plates 1 and 4). This S_1 increase results primarily from entrainment of PGW from layer 3 into layer 1 during both the Southwest and Northeast Monsoons. In addition, upwelling along the Omani coast during the Southwest Monsoon also brings saltier PGW into the surface layer, increasing S_1 by 0.1–0.2 psu there (lower panel of Figure 7b).

6.3. Pathways

The difference fields in Figure 7b illustrate pathways of PGW. After PGW enters the Indian Ocean in layer 3, it spreads slowly in the northern Arabian Sea, causing a strong horizontal salinity gradient. This spreading is primarily due to horizontal mixing and advection by the cyclonic circulation that is present in the northern Arabian Sea during most times of the year (see Figure 7a), even though it is weak. It is the northward branch of this cyclonic current that blocks PGW from spreading eastward and southward. In addition, entrainment during both monsoons and Omani coastal upwelling during the Southwest Monsoon help to remove part of the salty PGW from layer 3.

In the upper two layers most of the PGW is advected southward into the central Arabian Sea (lower panel of Figure 7b), and part of it flows back into the Persian Gulf with the ASW in the surface mixed layer. Thus almost all the PGW remains in the Arabian Sea in our solution, and only a small amount of it spreads into the rest of the basin. This result disagrees with the pathways suggested by *Rochford* [1964, Figure 23], who suggested that PGW spreads southward and bifurcates as it approaches the equator, with one branch continuing southward along the African coast and the other bending eastward along the equator to flow into the Bay of Bengal and eastern Indian Ocean. It is, however, consistent with a number of observational studies. *Kuksa* [1972] concluded that the influence of PGW is

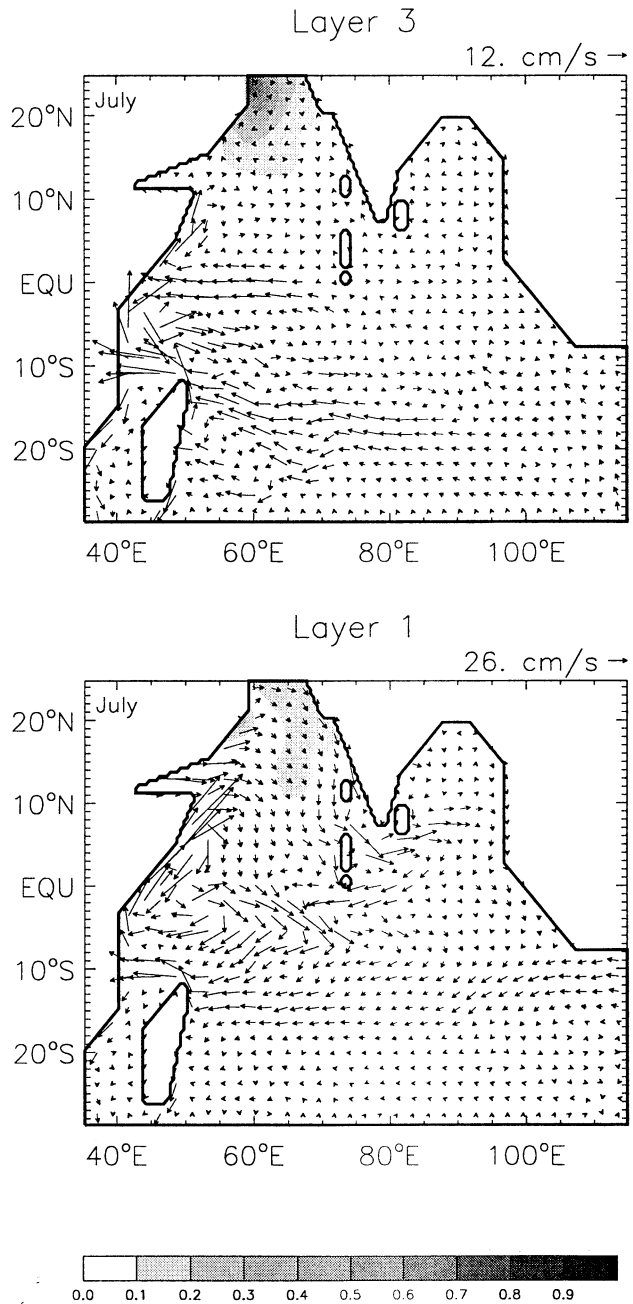

Figure 7b. Salinity fields from the difference solution, TR4 – TR3, and currents from solution TR4 for (top) layer 3 and (bottom) layer 1 during July. Salinity values are shaded, with an interval of 0.1 psu.

felt no farther south than 15°N. *Quadfasel and Schott* [1982] suggested that the boundary of PGW influence lies somewhere between 5°N and 10°N in the western Indian Ocean. *Morrison and Olson* [1991] concluded that PGW is rapidly mixed within the basin, noting that there is little evidence of this water mass south of 15°N except for isolated lenses.

7. Red Sea

7.1. Forcing

High-temperature (23°C) and high-salinity (39.5 psu) Red Sea Water (RSW) enters the Gulf of Aden from the lower section of the Bab el Mandab Strait, with an annual mean transport of approximately 0.3 Sv. Above this RSW inflow there is a corresponding Indian Ocean outflow returning to the Red Sea [*Osman*, 1985; *Maillard and Soliman*, 1986; *Johns, et al.*, 1998; *Murray*, 1998]. In the Gulf of Aden, RSW flows eastward mainly at depths of 400–700 m, undergoes vigorous mixing with its surrounding waters, and experiences double diffusion [*Fedorov and Meshchanov*, 1988]. Because of this mixing, the temperature and salinity of RSW change to 12°C and 36 psu near the mouth of the Gulf at 50°E, corresponding to a density of $\sigma_t = 27.25$, and its core is located at a depth of 600–700 m [*Rochford*, 1964; *Wyrtki*, 1971; *Quadfasel and Schott*, 1982; *Shapiro and Meshchanov*, 1991].

To model the inflow of RSW into the Indian Ocean, we specify an exchange circulation across the mouth of the Gulf of Aden. We modify the boundary conditions across the segment, $x = 50°\text{E}$, $11°\text{N} \le y \le 14.5°\text{N}$, to be

$$u_4 = \frac{M_4}{h_4 L_s}, \quad S_4 = S_{4\text{in}},$$
$$T_4 = T_{4\text{in}}, \quad u_1 = -\frac{M_1}{h_1 L_s}, \tag{6}$$

where $S_{4\text{in}} = 36$ psu, $T_{4\text{in}} = 12°\text{C}$, and $L_s = 3.5°$ is the width of segment. As discussed below, M_4 is set to 1.2 Sv because of mixing with the ambient waters in the Red Sea, and then M_1 follows from the salt balance equation across the segment

$$M_4 S_4 = M_1 S_1. \tag{7}$$

Values for $S_{4\text{in}}$ and $T_{4\text{in}}$ are suggested by observations at the mouth of the Gulf [*Shapiro and Meshchanov*, 1991].

Let $S_r = 39.0$ psu and $M_r = 0.3$ Sv represent salinity and mass transport of RSW out of the Bab el Mandab Strait, let $S_a = 35$ psu (obtained from solution TR4), and let M_a be the corresponding values of ambient water within the Gulf of Aden. Then, the salt and mass balances across the segment,

$$M_r S_r + M_a S_a = M_4 S_4,$$
$$M_r + M_a = M_4, \tag{8}$$

yield $M_4 = 4M_r = 1.2$ Sv.

7.2. Salinities

The upper panel of Figure 8 plots annual mean S_4 and $\mathbf{v}_4$ fields from the solution forced as in solution TR4 but also with inflow of RSW (TR5). Its lower panel shows the annual mean salinity field from the difference solution TR5 – TR4 and current from solution TR5 in layer 4. Except for the southeastern ocean the salty RSW increases S_4 throughout the Indian Ocean, especially in the Somali Basin where S_4 increases by 0.6–0.8 psu, and to a lesser extent in the Arabian Sea and the equatorial ocean (west of 90°E and north of 10°S), where S_4 is 0.1–0.6 psu saltier (upper panel of Figure 8). These

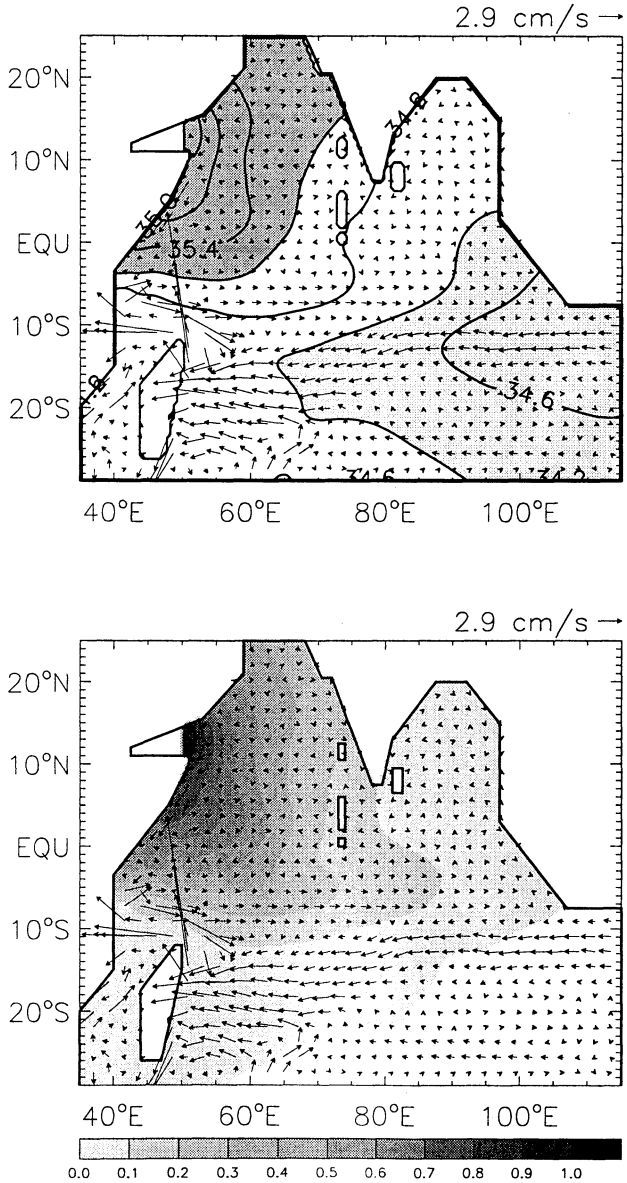

Figure 8. (top) Annual mean $\mathbf{v}_4$ field from solution TR5 overlying its annual mean S_4 field and (bottom) annual mean $\mathbf{v}_4$ field from solution TR5 overlying the annual mean S_4 from the difference solution TR5 – TR4. In the top panel the contour interval is 0.2 psu. Values greater than 35.2 psu have dark shading, and those smaller than 34.8 psu have lighter shading. In the bottom panel the shading interval is 0.1 psu.

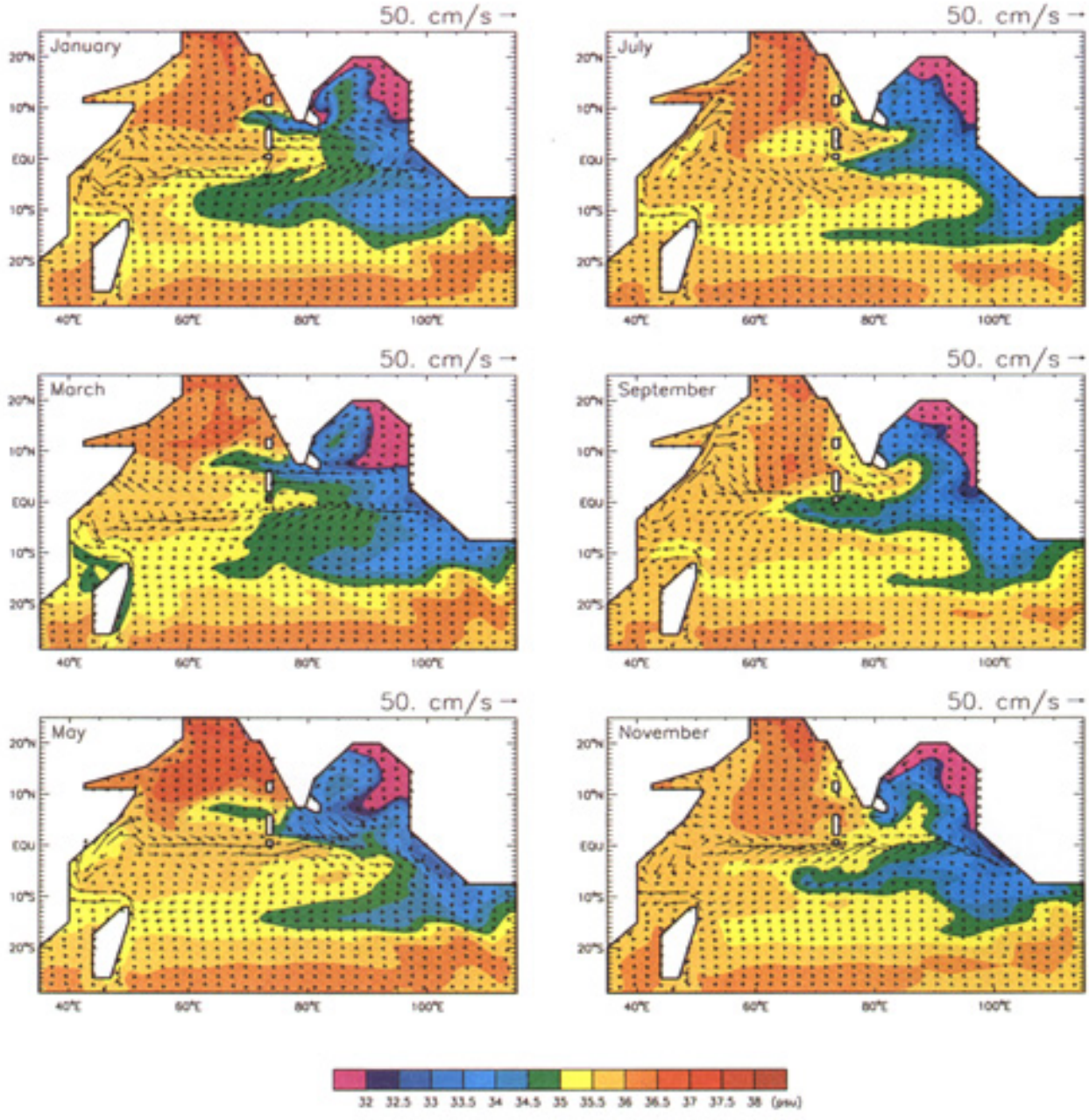

Plate 3a. Bimonthly plots of S_1 and $\mathbf{v}_1$ fields from solution TR2.

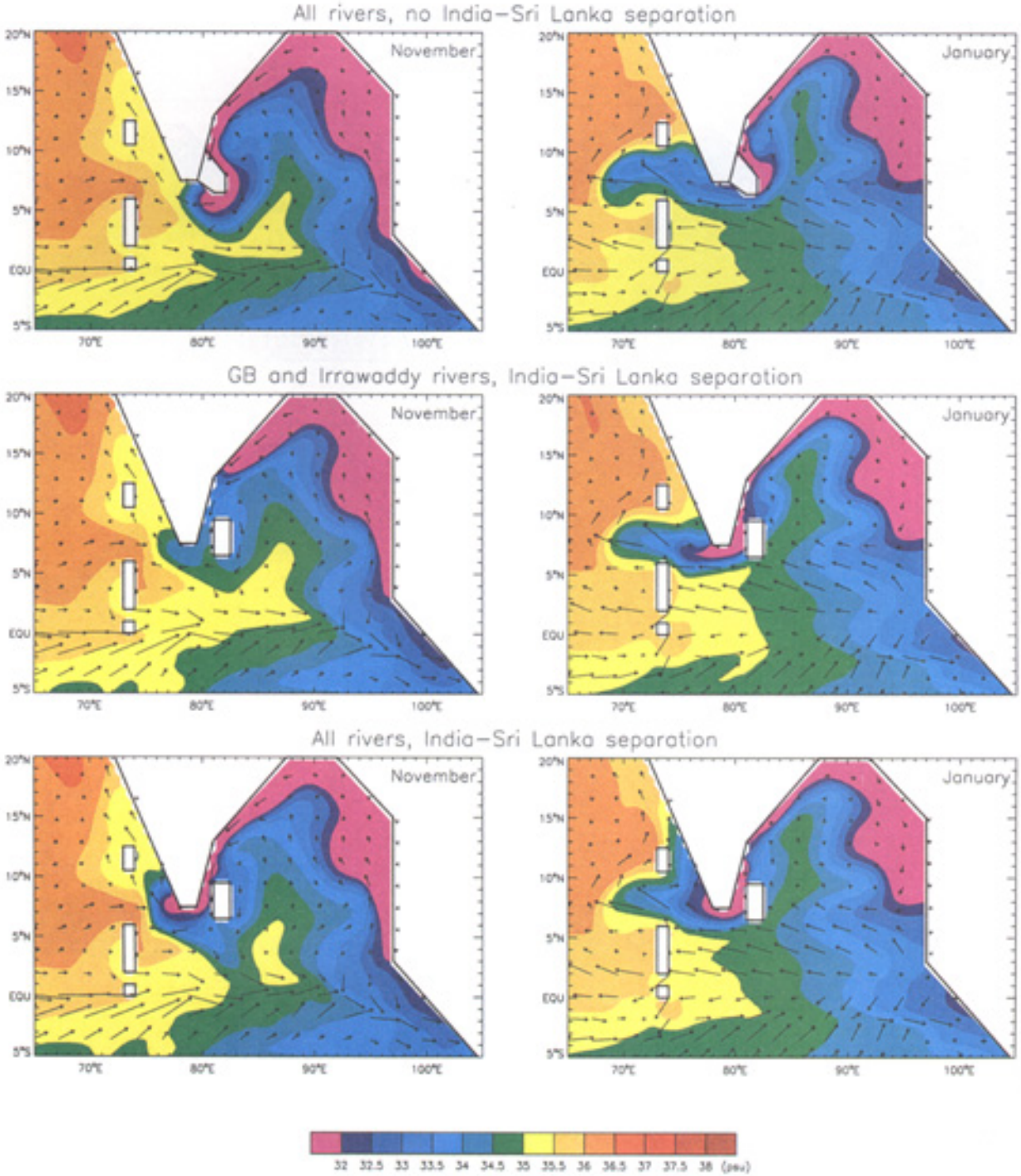

Plate 3b. Plots of S_1 and current $\mathbf{v}_1$ during November and January from solutions (top) TR2A, (middle) TR2B, and (bottom) TR2C. The vector scale for the current is the same as that in Plates 1, 2, and 3a.

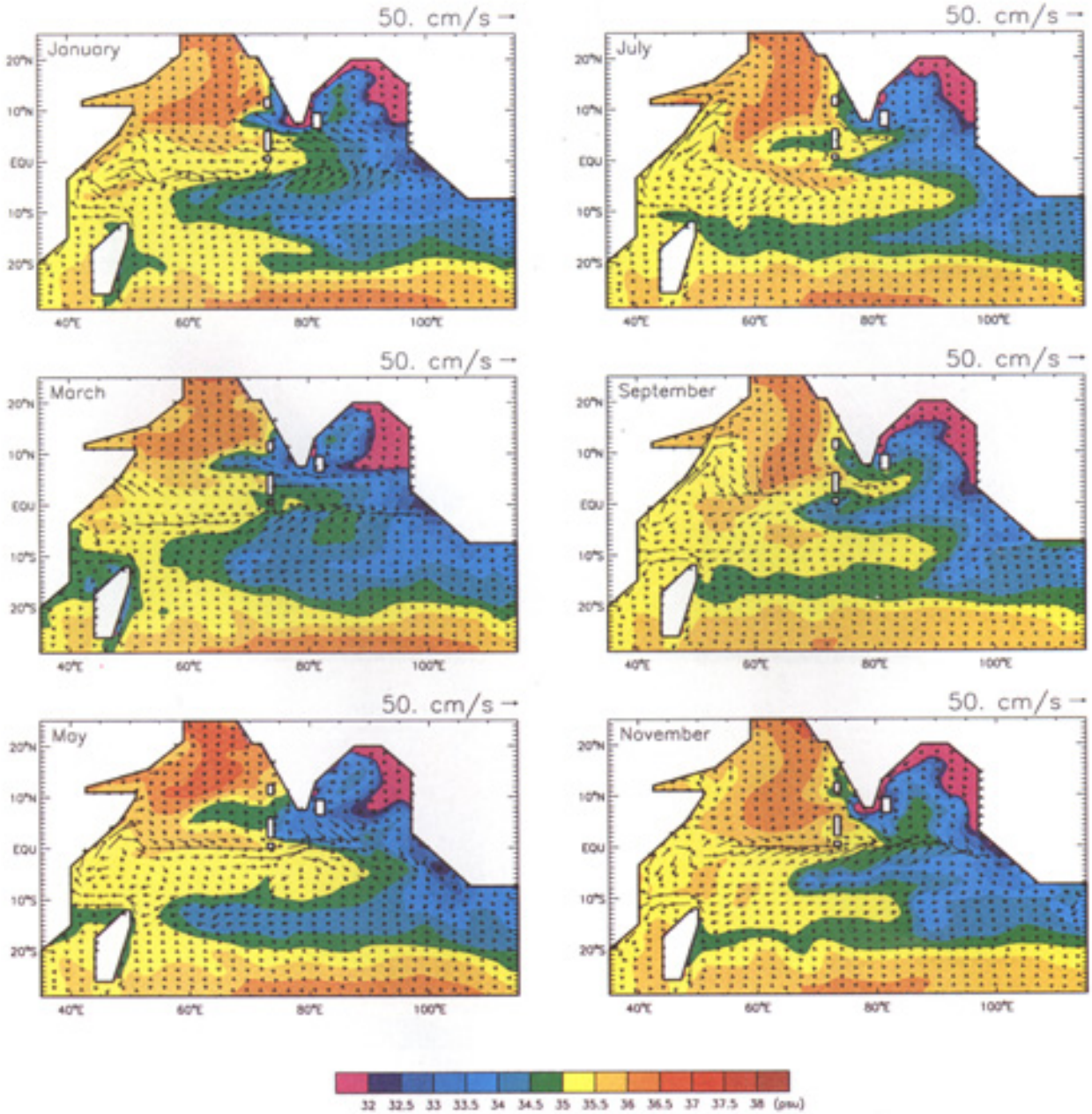

Plate 4. Bimonthly plots of S_1 and $\mathbf{v}_1$ fields from solution TR3.

features considerably improve annual mean S_4, making it agree much better with observations (bottom panel of Figure 6b). In the western ocean north of 5°S, however, observed isohalines are oriented east-west whereas in the solution they are north-south. This model-data discrepancy might result from the lack of data points near the coasts in the *Levitus and Boyer* [1994] data set. In support of the solution, *Quadfasel and Schott* [1982] reported the presence of high-salinity RSW along the Somali coast from 10°N to 5°S.

7.3. Pathways

The difference of S_4 fields (bottom panel of Figure 8) illustrates pathways of RSW more clearly. Immediately after RSW enters the Indian Ocean, it flows southward along the Somali coast due to coastal Kelvin waves forced by the RSW inflow. When RSW arrives at the equator, it spreads southward and eastward by mixing since currents are very weak in this region. Near 5°S the RSW is advected eastward, just north of the fresher Throughflow water. When the RSW arrives at 80°E, part of it spreads eastward to Sumatra and northward to the Bay of Bengal by advection and horizontal mixing. The rest mixes with the Throughflow water, returns to the western ocean within the westward flowing current, and finally flows out of the Indian Ocean in the southwestern region. In addition, RSW spreads over the northern Arabian Sea primarily because of horizontal mixing.

Generally, RSW pathways in the solution agree with the ones suggested by previous studies [*Rochford*, 1964; *Kuksa*, 1972; *Quadfasel and Schott*, 1982; *Grundlingh*, 1985; *Shapiro and Meshchanov*, 1991]. The exception is a pathway suggested by *Rochford* [1964, Figure 23] that extends southeastward across the equator and exits the Indian Ocean near the west Australian coast, a pathway that is completely missing in our solution. Considering that fresher water from the Antarctic Circumpolar Current is now known to enter the Indian Ocean in this region, this pathway might not be realistic.

8. Summary

In this study, we use a $4^1/_2$-layer model to investigate Indian Ocean salinity distributions caused by various forcings: $\mathcal{P}-\mathcal{E}$, Bay of Bengal river inflow, the Indonesian Throughflow, and exchange flows from the Persian Gulf and Red Sea. A suite of solutions is obtained in which these forcings are added sequentially, and the model salinity fields in layers 1, 3, and 4 are compared to observed *Levitus and Boyer* [1994] salinity fields at the sea surface, 200 m, and 600 m (Plate 1, Figure 3, and Figure 6b, respectively).

The solution forced only by $\mathcal{P}-\mathcal{E}$ (solution TR1) has an S_1 field that agrees qualitatively with observed SSS, generally being low in regions where $\mathcal{P}-\mathcal{E} > 0$ and high where $\mathcal{P}-\mathcal{E} < 0$ (Figure 2 and Plate 2), but overall values tend to be too high. Effects of advection are also evident: The spring and fall WJs generate high-salinity tongues in the equatorial ocean, the SEC causes a westward stretching, low-salinity tongue in the southern tropical ocean, the EICC and NMC carry the fresher Bay of Bengal water into the Arabian Sea, and the SMC and fall WJ bring saltier Arabian Sea water into the Bay of Bengal (Plates 1 and 2). In layer 3, subduction of surface water produces high S_3 in the Arabian Sea and southern tropical ocean near 20°S and low S_3 in the Bay of Bengal and in the Southern Hemisphere around 8°S (Figure 3).

The addition of fresh river water (solution TR2) considerably improves S_1, especially in the Bay of Bengal and along the west coast of India. During the first half of the Northeast Monsoon (November panel of Plate 3a), river water is advected around the perimeter of the Bay by a cyclonic circulation, forming a narrow plume along the east Indian coast due to southwestward advection by the EICC. Subsequently, it is carried into the interior of the Arabian Sea by the currents associated with the LH, where it mixes with the surrounding waters, and very little of it reaches the Somali coast (January and May panels of Plate 3a). Local rivers and a separation between India and Sri Lanka in layer 1 help to produce a wintertime, across-shelf salinity gradient along the west Indian coast (Plate 3b). During the Southwest Monsoon (July and September panels of Plate 3a) a southward current along the eastern boundary of the Bay carries a portion of the fresh water to the equator. Part of it is then advected westward near the equator; the rest flows southward across the equator to the southern tropical ocean and then it extends westward by the SEC. In layer 3, fresh water from the rivers decreases S_3 in the Bay of Bengal, near the west coast of India, and to a lesser extent, in a strip of the southern tropical ocean through subduction (compare Figures 3 and 5).

With the Indonesian Throughflow (solution TR3), fresher water extends westward in the SEC in the upper three layers, with a small portion flowing southward along the western Australian coast via the Leeuwin Current in layers 1 and 2. Most of the Throughflow flows out of the basin near Madagascar or along the western boundary. A significant amount, however, flows northward within the EACC, and then either eastward just south off the equator or northward into the Arabian Sea. Freshening by the Throughflow improves salinity distributions in layers 1–3, especially in the southern tropical ocean and the Arabian Sea (compare Plates 1, 3a, and 4 and Figures 3, 5, and 6a). In layer 4, Throughflow water flows across the basin only when its strength is increased from 1 to 6 Sv. Salinity S_4 agrees better with the *Levitus and Boyer* [1994] data in the latter case, suggesting that there is significant deep Throughflow transport in the real ocean or perhaps that horizontal mixing is too strong in our model.

Warmer and saltier water from the Persian Gulf enters the northwestern Indian Ocean in layer 3 (solution

TR4), forming a layer of PGW in the northern Arabian Sea that improves the salinity pattern there (Figures 3 and 7a). Consistent with the observations [*Quadfasel and Schott*, 1982; *Kuksa*, 1972; *Morrison and Olson*, 1991], most PGW stays in the Arabian Sea in this layer because currents are weak. A portion of it is carried into the upper two layers by entrainment during the Northeast and Southwest Monsoons, and to a lesser degree by upwelling along the Omani coast during the Southwest Monsoon. As a result, S_1 and S_2 increase by 0.1–0.2 psu in a broad region of the northern Arabian Sea, bringing S_1 even closer to observed values.

High-temperature and high-salinity RSW enters the Indian Ocean at the Gulf of Aden in layer 4 (solution TR5). It flows southward along the Somali coast due to coastal Kelvin waves forced by its mass influx (Figure 8), and near the equator it spreads southward and eastward primarily due to mixing since currents are weak in this region. It is advected eastward near 5°S, with part flowing all the way to Sumatra, part extending northward into the Bay of Bengal primarily by horizontal mixing, and the rest moving southward to join the westward flowing Indonesian Throughflow waters in layer 4. Salinity S_4 increases significantly in the northwestern portion of the basin, bringing it into much better agreement with the observations (Figures 8 and 6b).

In conclusion, we have shown that salinity distributions throughout the Indian Ocean can be simulated quite realistically, provided all the prominent forcing mechanisms are included. At the same time, there are some obvious differences between observed and modeled fields. These include S_1 being too fresh in the Bay of Bengal and the advection of Throughflow water and RSW being too weak in layer 4. These differences may result from model error (e.g., horizontal mixing being too large in layer 4). They may also result from errors in the forcing fields themselves. It will be difficult to make further progress until their accuracy is considerably improved.

Acknowledgments. This paper is based on Weiqing Han's thesis work, and she gratefully acknowledges the support of her committee members: Richard Dodge, Barry Klinger, Arthur Mariano, Robert Molinari, and Don Olson. We thank S. R. Shetye and D. Shankar for helpful suggestions and discussions and Kevin Kohler for his programming assistance. Thanks also go to the two anonymous reviewers for their constructive comments and suggestions. This research was supported by NSF through grants OCE-92-03916 and OCE-94-16098, by ONR through contract N00014-97-1-0077, and by the Frontier Research System for Global Change through its sponsorship of the International Pacific Research Center (IPRC). This manuscript is SOEST Contribution No. 5281 and IPRC Contribution No. 61.

References

Bray, N.A., S. Hautala, J. Chong, and J. Pariwono, Large-scale sea level, thermocline, and wind variations in the Indonesian Throughflow region, *J. Geophys. Res., 101*, 12,239–12,254, 1996.

Chao, S., T.W. Kao, and K.R. Al-Hajri, A numerical investigation of circulation in the Arabian Gulf, *J. Geophys. Res., 97*, 11,219–11,236, 1992.

Donguy, J.R., and G. Meyers, Seasonal variations of sea-surface salinity and temperature in the tropical Indian Ocean, *Deep Sea Res., Part I, 43*, 117–138, 1996.

Fedorov, K.N., and S.L. Meshchanov, Structure and propagation of Red Sea waters in the Gulf of Aden, *Oceanology, Engl. Transl., 28*, 357–363, 1988.

Fieux, M., C. Andrie, P. Delecluse, A.G. Ilahude, A. Kartartseff, F. Mantisi, R. Molcard, and J.C. Swallow, Measurements within the Pacific and Indian Oceans throughflow region, *Deep Sea Res., Part I, 41*, 1091–1130, 1994.

Fine, R.A., Direct evidence using tritium data for throughflow from the Pacific into the Indian Ocean, *Nature, 315*, 478–480, 1985.

Godfrey, J.S., A Sverdrup model of the depth-integrated flow for the world ocean allowing for island circulations, *Geophys. Astrophys. Fluid Mech., 45*, 89–112, 1989.

Godfrey, J.S., and T.T. Golding, The Sverdrup relation in the Indian Ocean and the effect of Pacific-Indian Ocean throughflow on Indian Ocean circulation and on the east Australian current, *J. Phys. Oceanogr., 11*, 771–779, 1981.

Gordon, A.L., Interocean exchange of thermocline water, *J. Geophys. Res., 91*, 5037–5046, 1986.

Grundlingh, M.L., Occurrence of Red Sea water in the southwestern Indian Ocean, *J. Phys. Oceanogr., 15*, 207–212, 1985.

Haines, M.A., R.A. Fine, M.E. Luther, and Z. Ji, Particle trajectories in an Indian Ocean model and sensitivity to seasonal forcing, *J. Phys. Oceanogr., 29*, 584–598, 1999.

Han, W., Influence of salinity on dynamics, thermodynamics, and mixed-layer physics in the Indian Ocean, Ph.D. dissertation, Nova Southeast. Univ., Dania, Fl., 147 pp., 1999.

Han, W., J.P. McCreary, D.L.T. Anderson, and A.J. Mariano, On the dynamics of the eastward surface jets in the equatorial Indian Ocean, *J. Phys. Oceanogr., 29*, 2191–2209, 1999.

Han, W., J.P. McCreary, and K.E. Kohler, Influence of precipitation-evaporation and Bay of Bengal rivers on dynamics, thermodynamics, and mixed-layer physics in the upper Indian Ocean, *J. Geophys. Res., In press*, 2000.

Hirst, A.C., and J.S. Godfrey, The role of Indonesian Throughflow in a global ocean GCM, *J. Phys. Oceanogr., 23*, 1057–1086, 1993.

Johns, W.E., S.P. Murray, and S.S. Sofianos, Atmospherically-forced exchange through the strait of Bab el Mandeb, *Eos Trans. AGU, 79*(1), Ocean Sci. Meet. Suppl., OS31O-3, 1998.

Kraus, E.B., and J.S. Turner, A one-dimensional model of the seasonal thermocline, II, The general theory and its consequences, *Tellus, 119*, 98–106, 1967.

Kuksa, V.I., Some peculiarities of the formation and distribution of intermediate layers in the Indian Ocean, *Oceanology, 12*(1), 21–30, 1972.

Kundu, P.K., and J.P. McCreary, On the dynamics of the throughflow from the Pacific into the Indian Ocean, *J. Phys. Oceanogr., 16*, 2191–2198, 1986.

Legates, D.R., and C.J. Willmott, Mean seasonal and spatial variability in gauge-corrected global precipitation, *Int. J. Climatol., 10*(2), 111–127, 1990.

Levitus, S., and T.P. Boyer, *World Ocean Atlas 1994*, vol. *1-4*, Natl. Oceanic and Atmos. Admin., Silver Spring, Md., 1994.

Maillard, C., and G. Soliman, Hydrography of the Red Sea and exchanges with the Indian Ocean in the summer. *Oceanolog. Acta, 9*, 249–269, 1986.

Mariano, A.J., E.H. Ryan, B.D. Perkins, and S. Smithers, The Mariano global surface velocity analysis 1.0, *USCG Rep.* CG-D-34-95, 55 pp., Res. and Devel. Cent., U. S. Coast Guard, Groton, Conn., 1995.

Martin, J.M., J.D. Burton, and D. Eisma Ed., *River Inputs to Ocean Systems*, U. N. Press, Switzerland, 384 pp., 1981.

McCreary, J.P., P.K. Kundu, and R.L. Molinari, A numerical investigation of dynamics, thermodynamics, and mixed-layer processes in the Indian Ocean, *Prog. Oceanogr., 31*, 181–224, 1993. (Erratum, *Prog. Oceanogr., 33*, 248, 1994.)

Meyers, G., R.J. Bailey, and A.P. Worby, Geostrophic transport of Indonesian Throughflow, *Deep Sea Res., Part I, 42*, 1163–1174, 1995.

Miyama, T., T. Awaji, K. Akitomo, and N. Imasato, Study of seasonal transport variations in the Indonesian Seas, *J. Geophys. Res., 100*, 20,517–20,541, 1995.

Miyama, T., T. Awaji, K. Akitomo, and N. Imasato, A Lagrangian approach to the seasonal variation of salinity in the mixed layer of the Indonesian Seas, *J. Geophys. Res., 101*, 12,265–12,285, 1996.

Molcard, R., and M. Fieux, The Indo-Pacific throughflow in the Timor Passage, *J. Geophys. Res., 101*, 12,411–12,420, 1996.

Morrison, J.M., and D.B. Olson, Seasonal basin wide extremes in T-S characteristics in the near surface waters of the Arabian Sea and Somali Basin, in *Oceanography of the Indian Ocean*, pp. 605-616, Oxford and IBH, New Delhi, 1991.

Murray, S.P., Two years of observations of the seasonal cycle of transport through the Bab el Mandeb strait, *Eos Trans. AGU, 79*(1), Ocean Sci. Meet. Suppl., OS31O-1, 1998.

Murray, S.P., and D. Arief, Throughflow into the Indian Ocean through the Lombok strait, January 1985-January 1986, *Lett. to Nature, 333*, 444–447, 1988.

Murty, V.S.N., R.V.B. Sarha, D.P. Rao, and C.S. Murty, Water characteristics, mixing and circulation in the Bay of Bengal during Southwest Monsoon, *J. Mar. Res., 50*, 207–228, 1992.

Osman, M.M., Water exchange between the Red Sea and Gulf of Aden, *International Symposium on the Most Important Upwelling Areas off Western Africa*, vol. *1*, pp. 205–212, Inst. of Inv. Resq., Barcelona, Spain, 1985.

Quadfasel, D.R., and F. Schott, Water-mass distributions at intermediate layers off the Somali coast during the onset of the southwest monsoon, 1979, *J. Phys. Oceanogr., 12*, 1358–1372, 1982.

Reynolds, R.M., Physical oceanography of the Gulf, strait of Hormuz, and the Gulf of Oman-results from the Mt. Mitchell Expedition, *Mar. Pollut. Bull., 27*, 35–59, 1994.

Rochford, D.J., Salinity maxima in the upper 1000 meters of the north Indian Ocean, *Aust. J. Mar. Freshwater Res., 15*, 1–24, 1964.

Shankar, D., and S.R. Shetye, On the dynamics of the Lakshadweep High and Low in the southeastern Arabian Sea, *J. Geophys. Res., 102*, 12,551–12,562, 1997.

Shapiro, G.Z., and S.L. Meshchanov, Distribution and spreading of the Red Sea water and salt lens formation in the northwest Indian Ocean, *Deep Sea Res., 38*, 21–34, 1991.

Shetye, S.R., The movement and implications of the Ganges-Brahmaputra run off on entering the Bay of Bengal, *Curr. Sci., 64*(1), 32–38, 1993.

Shetye, S.R., A.D. Gouveia, S.S.C. Shenoi, G.S. Michael, D. Sundar, A.M. Almeida, and K. Santanam, The coastal current off western India during the Northeast Monsoon, *Deep Sea Res., 38*, 1517–1529, 1991.

Shetye, S.R., A.D. Gouveia, D. Shankar, S.S.C. Shenoi, P.N. Vinayachandran, D. Sundar, G.S. Michael, and G. Nampoothiri, Hydrography and circulation of the western Bay of Bengal during the Northeast Monsoon, *J. Geophys. Res., 101*(C6), 14,011–14,025, 1996.

United Kingdom Hydrographic Office, *West Coast of India Pilot*, 11th ed., London, 1975.

United Nations Educational, Scientific, and Cultural Organization (UNESCO), Discharge of selected rivers of the world, general and regime characteristics of stations selected, *Stud. Rep. Hydrol. 5*, vol. *1*, 70 pp., Paris, 1972.

United Nations Educational, Scientific, and Cultural Organization (UNESCO), Discharge of selected rivers of the world, mean monthly and extreme discharges (1969-72), *Stud. Rep. Hydrol., 5*, vol. *3*, part 2, 124 pp., Paris, 1974.

United Nations Educational, Scientific, and Cultural Organization (UNESCO), Discharge of selected rivers of the world, mean monthly and extreme discharges (1972-1975), *Stud. Rep. Hydrol., 5*, vol. *3*, part 3, 104 pp., Paris, 1979.

United Nations Educational, Scientific, and Cultural Organization (UNESCO), River inputs to ocean systems: Status and recommendations for research, Final report of SCOR Working Group 46, Edited by J.D. Burton., *UNESCO Tech. Pap. Mar. Sci., 55*, 26 pp., Paris, 1988.

Vinayachandran, P.N., Y. Masumoto, T. Mikawa, and T. Yamagata, Intrusion of the Southwest Monsoon Current into the Bay of Bengal, *J. Geophys. Res., 104*, 11,077–11,085, 1999.

Wyrtki, K., Physical oceanography of the southeast Asian waters, *NAGA Rep. 2*, 195 pp., Scripps Inst. of Oceanogr., La Jolla, Calif., 1961.

Wyrtki, K., *Oceanographic Atlas of the International Indian Ocean Expedition*, Nat. Sci. Found., Washington, D. C., 531 pp., 1971.

Wyrtki, K., An equatorial jet in the Indian Ocean, *Science, 181*, 262–264, 1973.

W. Han, Program in Atmospheric and Oceanic Sciences, University of Colorado, Campus Box 311, Boulder, CO 80309. (whan@monsoon.colorado.edu)

J.P. McCreary, International Pacific Research Center, School of Ocean and Earth Science and Technology, University of Hawaii, 2525 Correa Road, Honolulu, HI 96822. (jay@iprc.soest.hawaii.edu)

(Received March 21, 2000; revised August, 28, 2000; accepted September 13, 2000.)